Lateral Load Testing of the Advanced Stirling Convertor (ASC–E2) Heater Head

Peggy A. Cornell[1] and David L. Krause[2]
NASA Glenn Research Center, Cleveland, Ohio, 44135

Glen Davis[3]
Sunpower, Inc., Athens, Ohio, 45701

Malcolm G. Robbie[4] and David A. Gubics[5]
QinetiQ North America, Cleveland, Ohio, 44135

Free-piston Stirling convertors are fundamental to the development of NASA's next generation of radioisotope power system, the Advanced Stirling Radioisotope Generator (ASRG). The ASRG will use General Purpose Heat Source (GPHS) modules as the energy source and Advanced Stirling Convertors (ASCs) to convert heat into electrical energy, and is being developed by Lockheed Martin under contract to the Department of Energy. Achieving flight status mandates that the ASCs satisfy design as well as flight requirements to ensure reliable operation during launch. To meet these launch requirements, GRC performed a series of quasi-static mechanical tests simulating the pressure, thermal, and external loading conditions that will be experienced by an ASC–E2 heater head assembly. These mechanical tests were collectively referred to as "lateral load tests" since a primary external load lateral to the heater head longitudinal axis was applied in combination with the other loading conditions. The heater head was subjected to the operational pressure, axial mounting force, thermal conditions, and axial and lateral launch vehicle acceleration loadings. To permit reliable prediction of the heater head's structural performance, GRC completed Finite Element Analysis (FEA) computer modeling for the stress, strain, and deformation that will result during launch. The heater head lateral load test directly supported evaluation of the analysis and validation of the design to meet launch requirements. This paper provides an overview of each element within the test and presents assessment of the modeling as well as experimental results of this task.

Nomenclature

AFSPCMAN	=	Air Force Space Command Manual
ASC	=	Advanced Stirling Convertor
ASRG	=	Advanced Stirling Radioisotope Generator
CSAF	=	Cold Side Adapter Flange
FEA	=	Finite Element Analysis
GPHS	=	General Purpose Heat Source
GRC	=	Glenn Research Center
LVDT	=	Linear Variable Differential Transformer
PIR	=	Program Information Request/Release
RPS	=	Radioisotope Power System

[1]Test Engineer, GRC–RPT, 21000 Brookpark Rd/Mail Stop 301–2, AIAA Member.
[2]Research Materials Engineer, GRC-RXL, 21000 Brookpark Rd/Mail Stop 51–1, AIAA Member.
[3]Mechanical Engineer, Sunpower, Inc., 182 Mill Street, Athens, OH 45701.
[4]Design Engineer, QinetiQ North America, 21000 Brookpark Rd/Mail Stop 500–AOS.
[5]Mechanical Engineer, QinetiQ North America, 21000 Brookpark Rd/Mail Stop 500–AOS.

I. Introduction

NASA's next generation of Radioisotope Power System (RPS), the Advanced Stirling Radioisotope Generator (ASRG), is progressing toward flight qualification. It is intended to provide electrical power for spacecraft and planetary probes that cannot rely on solar energy. The ASRG system efficiency of 28 to 32% would reduce the amount of radioisotope required for a given power level by a factor of four compared to radioisotope thermoelectric generators. Its high specific power enables certain missions and applications.[1]

A key element in the path to qualification is that the Advanced Stirling Convertors (ASCs) satisfy design as well as flight requirements that achieve reliable operation during launch. The ASCs are being developed by Sunpower, Inc. under the management and technical assistance of NASA Glenn Research Center (GRC). One of the requirements for launch mandated from the Air Force Space Command Manual (AFSPCMAN) 91–710 V3 was fulfilled by subjecting an ASC–E2 heater head assembly to the maximum external axial and lateral loads anticipated during an ASRG mission and verifying that it successfully withstood the load environment. The load values and load application points for this test were documented by Lockheed Martin in the Program Information Request/Release (PIR) for derivation of loads to be used for the heater head lateral load test. A secondary objective of this test was to qualify the Finite Element Analysis (FEA) used to predict the stress, strain, and deflection within the test article. The heater head lateral load test subjected the hardware to thermal, pressure, and external force loads, while measuring the stress, strain, and deflection at key locations of interest.

II. Test Description

A. Test Article

The test article used to qualify the heater head analysis and to provide validated test results to meet launch requirements was an ASC–E2 assembly prepared and provided by Sunpower, Inc., of Athens, Ohio. The test article is shown in Fig. 1 and consists of the following major components: heater head assembly, transition assembly, cylinder assembly, pressure vessel, split flange, water jacket assembly, load block, and deflection plates.

The heater head assembly consists of the heater head, heat collector body, heater collector plate, and internal acceptor. The heater head assembly was fabricated and tested according to Sunpower, Inc's ASC–E2 process document with the exception of bolt holes that were placed in the heat collector plate and heat collector body. The purpose of the bolt holes was for attachment of the load block and upper deflection plate unique to this test. The load block was fabricated and mounted above the heat collector to permit both axial loading through the test article axis and lateral loading through a line of action simulating the combined center of gravity of components above the cold side adapter flange (CSAF). The upper and lower deflection plates were used for mounting the mini-LVDTs (Linear Variable Differential Transformers) to measure lateral deflection and rotation.

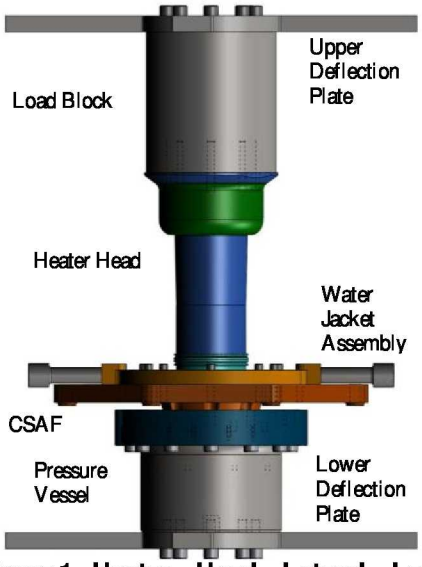

Figure 1. Heater Head Lateral Load Test Article. *3-D model of the primary assembly components.*

The transition assembly, which was secured to the heater head assembly by laser welding the weld flange on the heater head to the flange on the transition, consists of the transition, internal rejector, external rejector, and CSAF. The internal and external rejectors were brazed to the transition, while the CSAF was attached to the external rejector by electron beam welding. A water jacket assembly was fixed firmly to the top side of the CSAF and was used to control the rejector temperature of the test article. The water jacket assembly contains an integral, open channel for heated glycol to be brought into contact with the CSAF. The transition assembly as a whole was then joined via a split flange to the pressure vessel that held the lower deflection plates.

The cylinder assembly, which extends into the bore of the heater head, comprised a cylinder, hot cylinder, clamping ring, and regenerators. The cylinder was modified from the baseline ASC–E2 design to allow for a pressure vessel of shorter length. The pressure vessel was designed specifically to fit over the opening to the cavity in the heater head permitting pressurization of the test article. A full-scale pressure vessel was unnecessary given

that the linear alternator and related components were not required for assessment of the structural performance of the heater head.

B. Test Fixtures and Hardware

A preexisting test fixture was used to mount the ASC–E2 heater head and instrumentation. The rigid fixture provided support and alignment for the test article and provided the datum for displacement measurements. The fixture was mounted to the test facility bedplate and allowed access to the test article for load actuators, LVDTs, strain gages, heating source, and pressurization system. The components that made up the fixture include mini-LVDT displacement sensors, LVDT mounting plates and brackets, load rollers, and a mounting plate and stands. Sunpower, Inc. was responsible for designing and fabricating a new mounting plate and stands customized for testing the ASC–E2 test article. The remaining preexisting components were employed without modification. A view of the test article mounted onto the fixture's mounting plate is shown in Fig. 2. The test article CSAF was bolted to the mounting plate. Stiff plates enclosed the test article and provided attachment locations for the mini-LVDTs, as well as provided a level of protection for test personnel from potential burn and burst hazards.

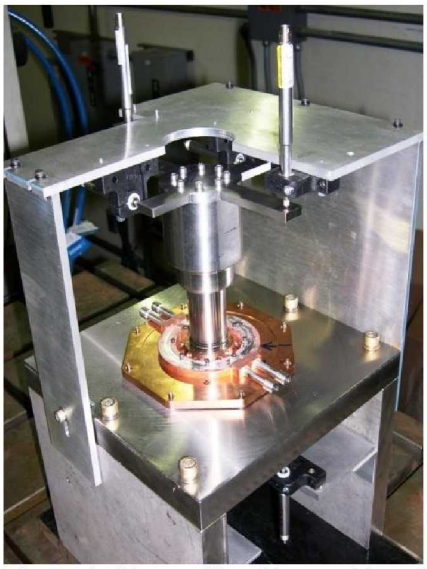

Figure 2. Heater Head Lateral Load Test Article mounted onto the fixture's rigid mounting plate.

C. Test Machine and Instrumentation

As shown in Fig. 3, an Instron in-plane biaxial load frame at the NASA GRC Structural Benchmark Test Facility was used to apply external loads to the test article using servo-valve-controlled hydraulic actuators. The stiffness of the load frame was designed to industry standards for high-cycle fatigue loadings up to 200,000 pounds. The four axes' positions are actuated with 110,000-pound-capacity double-acting hydraulic pistons. Closed-loop stroke displacement control of the actuators was achieved with feedback from LVDTs mounted inside the actuators' hydraulic pistons. Closed-loop load control was achieved with feedback from 2500-pound-capacity fatigue-rated load cells mounted to each actuator. To accommodate the ASC–E2 Heater Head Lateral Load Test, a custom bedplate was installed within the load frame, which included a top 5-inch-thick T-slotted steel mounting plate rigidly attached vertically and horizontally to the load frame.

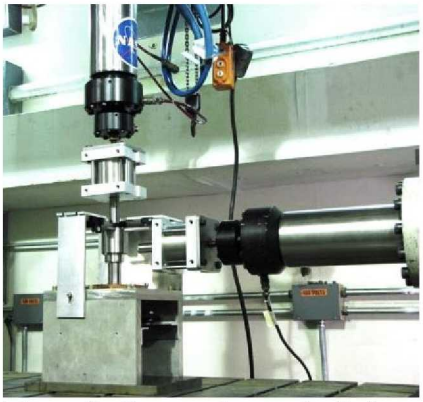

Figure 3. Servo-valve-controlled hydraulic actuators in the Instron in-plane biaxial load frame. *The actuators were used to apply external loads to the test article.*

Control of the load frame actuators was accomplished with an MTI TESTExpress Biaxial Digital Controller, Version 1.0.17 (2009). This controller provides programmable proportional-integral-derivative closed-loop stroke, load, or strain control of the actuator motion. Actuator control can be independent, or linked in any combination including cross-compensated centroidal control. A function generator is also provided to permit preprogramming of loading waveforms for each actuator. Furthermore, limit stop and annunciation functionality is provided to safely terminate any loading upon reaching a predefined load or displacement limit. The load frame controller, which was powered by an uninterruptible conditioning power supply, also includes a basic data acquisition system to record the applied loads and displacements from the four actuators, plus eight additional channels for conditioned analog signals such as strain gages or LVDTs.

Bimba Flat-1 Model FS–1252.5 pneumatic cylinders were used on the load frame actuators to provide a mechanical overload safety function. They were powered by the laboratory central service air system and controlled locally with Marsh Bellofram Type 10EXHR–REG–25–2–120T10 high relief exhausting regulating valves.

For controlling and maintaining the test article's temperature, an ethylene glycol solution was pumped to the test article water jacket with a Fisher Scientific Isotemp 3016 recirculation water heating-cooling bath. For controlling and maintaining the test article's internal pressure, a K-bottle helium source was manually controlled with a gas regulator; the system included a spring-loaded relief valve set to protect the assembly from over-pressurization.

A National Instruments LabVIEW 5.01 data system was used to collect and save the test data. The collection rate is programmable and was synchronized with the load frame controller. The channels that were acquired include four

load and two stroke channels from the load frame controller; eight mini-LVDTs; and 18 strain gages. A National Instruments SCXI data conditioning system was used to stream the digital data, including load, stroke, mini-LVDT, and strain gage signals, to the LabVIEW system. Other test data were primarily static and recorded by hand. This information included test article dimensional data, test article internal pressure, glycol bath reservoir, test article rejector temperature, room temperature, room relative humidity, and actuator air cylinder pressures.

The axial and lateral loads were controlled and measured using two 2,500-pound-capacity Tovey Model FR10–2.5K–B000 load cells. Loads were also measured redundantly with two 12,500-pound-capacity Tovey Model FR20–12.5K–B000 load cells mounted in series on the actuator. The loads cells were conditioned by the load frame controller system that also provided analog output signals. The analog signals were converted to digital signals by a National Instruments module in the test data acquisition system. The axial and lateral load locations on the test article are shown in Fig. 4.

A Noshok Model 615–1000–2–1–2–8 pressure transducer and digital readout measured the internal pressure. Two Omega Type N thermocouples measured the test article rejector temperature through thermocouple access holes with a Fluke Model 54II handheld conditioner. The pressure and temperature readings were recorded by hand.

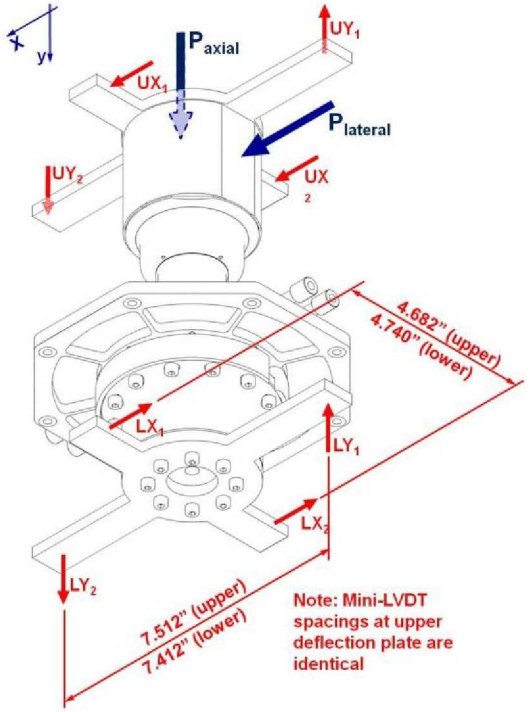

Figure 4. Heater Head Lateral Load Test Article load and mini-LVDT locations.

The test article displacements were measured by eight Micro-Epsilon DTA–1G–1.5–SA–F mini-LVDTs. These were conditioned with matched Micro-Epsilon in-line conditioners that provided analog output signals, which were converted to digital signals by National Instruments modules in the data acquisition system. As shown in Fig. 4, the mini-LVDTs were located on the upper and lower deflection plates, denoted by "U" and "L," and representing "X" and "Y" axes, respectively. For the upper deflection plate located on top of the load block, two mini-LVDTs were mounted laterally and measured lateral deflection and rotation. The average of the two displacement readings is the lateral deflection of the point midway between the measurement points, and their difference divided by their separation distance is the torsional rotation of the line connecting their centers. Two mini-LVDTs were mounted axially on the upper deflection plate and measured axial deflection and rotation. The average of the two displacement readings is the axial deflection of the point midway between the measurement points, and their difference divided by their separation distance is the bending rotation of the line connecting their centers. Four mini-LVDTs were mounted on the lower deflection plate located beneath the pressure vessel and measured deflections and rotations similarly. Comparison of deflection and rotation of the upper and lower plates provided an evaluation of linearity and elasticity of the test article and discernment of distortion between the heater head and the CSAF.

Two Vishay Micro-Measurements Type EA–06–062AA–120 strain gages, one trimmed Type EA–06–031RB–120, and five Type EA–06–031RB–120 strain gage three-element rectangular rosettes permitted measurement of 18 test article strains. Four three-element strain gage rosettes were located near the predicted highest stress area on the MarM-247 heater head test article and provided the surface two-dimensional state-of-strain through standard mechanics of materials strain

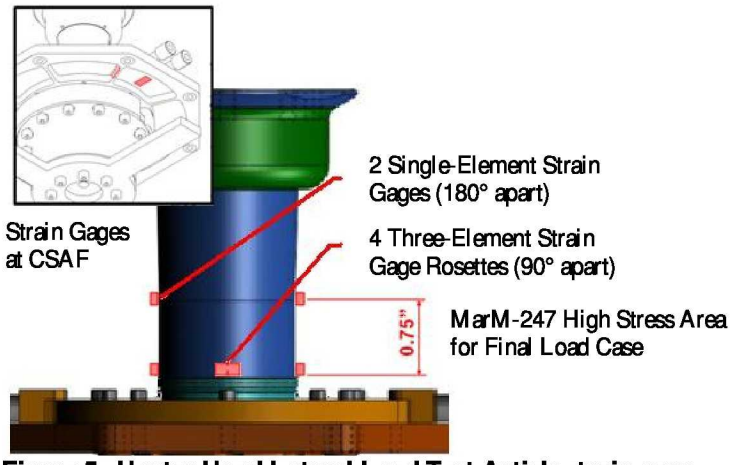

Figure 5. Heater Head Lateral Load Test Article strain gage locations.

equations. Two single-element strain gages measured principal strains at the predicted high stress area slightly removed from geometry-induced stress concentrated areas. Additionally, one rosette and one single-element gage measured strains in the CSAF component. National Instruments modules in the test data acquisition system conditioned the thermocouple readings. The strain gage locations on the test article are shown in Fig. 5.

D. Test Methodology

A substitute test article with dimensions and stiffness similar to the heater head was used to determine acceptable proportional-integral-derivative settings for the test frame closed-loop controller. This assured that the axial and lateral load hydraulic actuators would provide stable, acceptable performance for testing in load control. Representative ramped load steps of the test sequence matrix were applied to the substitute test article to assure proper operation of controls, instrumentation, and data recording. Finally, the substitute test article was used to activate the actuator push-rods to determine correlation factors for the overload safety pneumatic cylinders, which relate air pressure to mechanical overload force protection. The substitute test article was removed and the heater head test article and all related instrumentation was installed and verified. Alignment of the heater head test article within the load frame was determined by observation of strain gage readings upon axial loading to 50 pounds.

The heater head test article was tested in three combined external load cases. Each case required 100 °C temperature at the rejector braze location and the maximum internal operating pressure expected during launch. For each load case, the axial or lateral external loads were applied in discontinuous increasing and decreasing ramped steps of increasing peak magnitude until the maximum indicated peak load value was reached. This enabled structural evaluation of the test article for evidence of material yielding or other failure modes during and after each ramp step. The temperature and pressure conditions as well as the following loads were provided by the Lockheed Martin PIR.

1. Load Case 1 – Maximum expected flight axial compressive load
2. Load Case 2 – Nominal flight axial load plus maximum expected flight lateral load
3. Load Case 3 – Nominal flight axial load plus failure-inducing lateral load

For Load Case 1, the peak values of the axial ramped steps were increased incrementally until the indicated peak load was reached. For Load Case 2, the peak values of the lateral ramped steps were increased incrementally until the indicated peak load was reached. For Load Case 3, the alternating ramped steps of increasing peak magnitude concluded with a steady lateral load ramp that was imposed on the test article until a failure-inducing lateral load was reached. Failure was defined in the test plan by the first occurrence of significant material yielding, material stress rupture, elastic or inelastic buckling, braze failure, fastener fracture, or leakage of the pressurization gas.

III. Analysis

Pro/Engineer was utilized with ANSYS simulation software for stress, strain, and deflection predictions of the three load cases. The geometry was updated based on measurements obtained from the test article inspection report provided by Sunpower, Inc. This allowed for "as-built" configuration geometries of the test article and the test fixture to provide the baseline modeling data for this analysis. The parameters for each of the load case simulations were provided by Lockheed Martin. Simulations were based on the test conditions of maximum internal operating pressure, however, the thermal conditions were analyzed at room temperature rather than operating temperature. This thermal state was acceptable for the analysis given that the behavior of MarM-247 material tends to exhibit similar property characteristics at temperatures less than 800 °C. The boundary conditions for the load cases were set by fixing the model on eight mounting locations on the CSAF. For Load Case 1, the maximum compressive axial force anticipated during a mission was applied to the top of the load block. For Load Case 2, a compressive axial force of reduced intensity as well as the maximum anticipated lateral force was applied to the load block through a line of action simulating

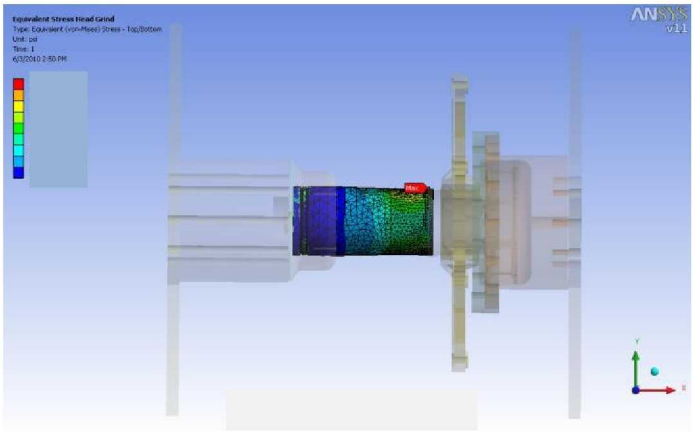

Figure 6. Predicted Maximum Stress in Heater Head. *The red arrow indicates the maximum stress location on the test article given an applied lateral load.*

the combined center of gravity above the CSAF. Load Case 3 was equivalent to Load Case 2 with the exception of an increased lateral load to the point of yield on the heater head. Figure 6 shows the location of predicted maximum stress on the heater head for Load Cases 2 and 3, and thus the location of predicted failure in Load Case 3.

Furthermore, deflection values of the upper and lower deflection plates for each load case in the model were determined by ANSYS and used to generate the predicted lateral deflection and rotation of the test assembly.

This predicted force and deflection data was used during the actual test to corroborate the experimental results.

IV. Experimental Results

A. Pre-Test Configuration

Prior to applying the external loads, the test article was heated to 100 °C at the rejector braze location by pumping an ethylene glycol solution of higher temperature to the test article water jacket and maintaining a temperature gradient such that the rejector braze location reached the required 100 °C. Upon reaching thermal equilibrium, the test article was pressurized internally with helium gas at the specified maximum operating pressure, which was maintained by manually regulating a K-bottle helium source. Strain measurements at predicted high stress areas indicated that the strain at this state was nominal.

B. Material Inelasticity Description

MarM-247 does not have a well-defined yield point like materials such as carbon steel. Rather, upon first loading, an initially stiff linear stress-strain response gradually transforms to lower values until the ultimate strength is attained. For such metals, the ASTM Standard E6 is often used to define the yield strength for the material at a particular offset strain value, commonly 0.2%. The curve denoted "Tensile Test Data" in Fig. 7 illustrates the stress-strain behavior, and the dashed lines show the determination of the yield strength (0.2% offset) from the intersection of a line parallel to the initial tangent modulus line and offset to +0.2% strain.

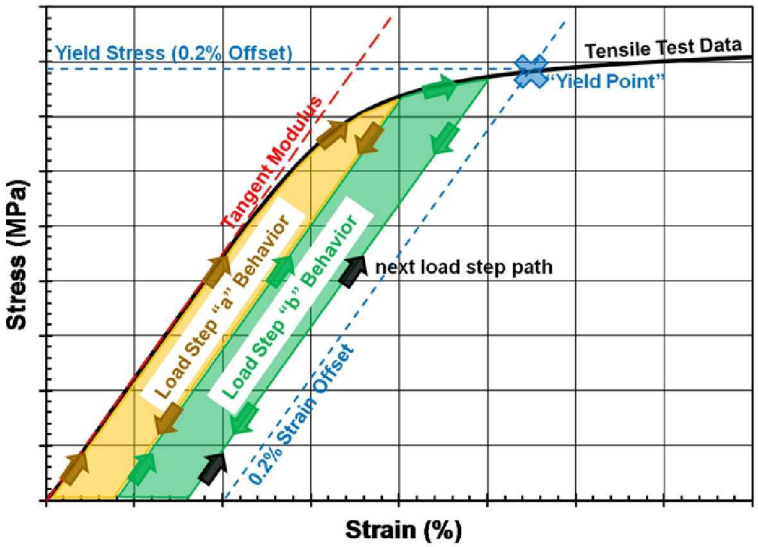

Figure 7. Strain Hardening Illustration. *The incremental accumulation of inelastic strain during cyclic increasing load steps is illustrated on a stress-strain diagram for a generic material with an indistinct yield point; linear behavior is manifest for load magnitudes up to the prior loading history.*

When such a material is loaded as was performed for the heater head lateral load test, the cyclic increasing load steps result in the incremental accumulation of inelastic strain. At stress levels previously not experienced, the nonlinear stress-strain curve is followed; at stress levels at or below prior loading history, the deformation is linear and occurs at the initial tangent elastic modulus. Steps of unloading follow the elastic modulus, but are offset by the amount of inelastic (plastic) strain. Two increasing load steps are shown, for example, in yellow and green in Fig. 7. The designation of the "Yield Point" has no effect on this deformation pattern, but rather is chosen to facilitate engineering design of structures using such materials.

C. Load Case 1

The first four axial load ramps of Load Case 1 were completed without incident, except that the measured axial deflections, although very small in magnitude, greatly exceeded the predicted values. For this reason, it was decided to perform the Load Case 2 lateral load ramps before proceeding with the final two axial load ramps of Load Case 1. After completing Load Case 2, these final two axial load ramps were completed without incident. The load-time history for Load Case 1 is shown in Fig. 8.

Figure 9 shows the measured axial deflections relative to axial load. The average axial deflections were measured from the "Y" axis of the upper and lower deflection plates (shown in Fig. 4), denoted by "UY" and "LY". The small difference in peak values recorded for the upper and lower deflection plates indicates that the majority of the deformation occurred in the CSAF. Resolution of the discrepancy between predicted and measured axial deflections is ongoing. With the displacements and longitudinal strains (Fig. 10) showing linear behavior and post-ramp values returning to the initial state, it was apparent that yielding did not occur under Load Case 1. For Fig. 10 and the remaining longitudinal strain figures, the lateral load was applied at the 000 location and the strain measurement locations are represented in a counter-clockwise direction from the top view. "U" and "L" represent the upper and lower strain gage placements (shown in Fig. 5). The test article did not exhibit yielding, stress rupture, elastic buckling, braze failure, fastener fracture, leakage of the internal helium gas, or any other failure mode in Load Case 1. It was determined that the test article passed the ASRG maximum expected mission axial load test requirement.

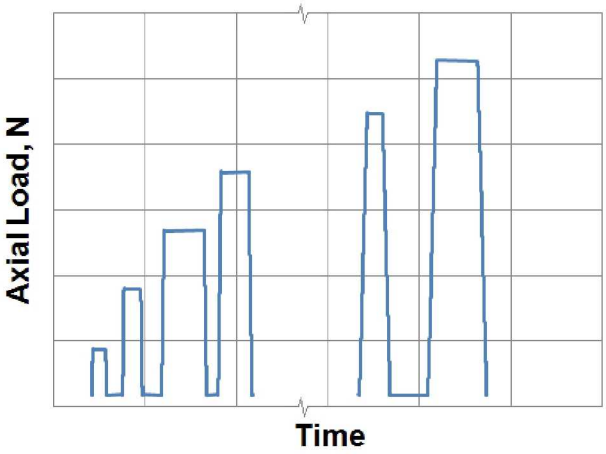

Figure 8. Load Case 1 Time History. *This plot shows application of constant rate axial load ramps with variable inspection hold times at loaded and unloaded states for the Load Case 1 loading sequence; the final ramp shown is the maximum expected mission axial load.*

D. Load Cases 2 and 3a

After application of the maximum mission axial compressive load, the five lateral load ramps of Load Case 2 proceeded as planned (Fig. 11). For loads up to the maximum of Load Case 2, the measured test article lateral deflections (Fig. 13), lateral rotations (Fig. 14), and longitudinal strains (Fig. 15) closely matched predicted values, were linear, and returned to their initial states upon unloading, as indicated in the plots shown by heavy bold lines. Similar to Load Case 1, yielding, stress rupture, elastic buckling, braze failure, fastener fracture, leakage of the internal helium gas, and other failure modes did not occur in Load Case 2. It was determined that the test article passed the ASRG maximum expected mission lateral load test requirement.

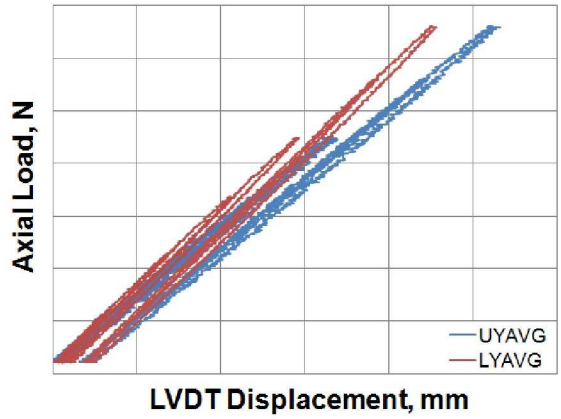

Figure 9. Load Case 1 Measured Axial Deflections. *Though larger than predicted, the axial deflections still create apparently noisy data plots due to their small magnitude; inelastic behavior is minimal. Angular displacements were imperceptible from electronic noise.*

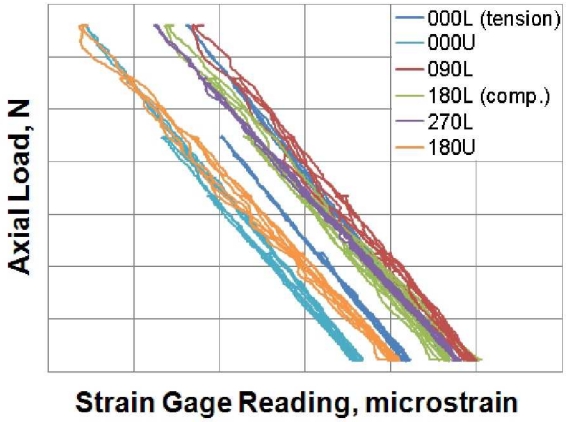

Figure 10. Load Case 1 Measured Longitudinal Strains. *The positive-valued longitudinal strains due to internal pressure were decreased during the compressive axial loadings of Load Case 1.*

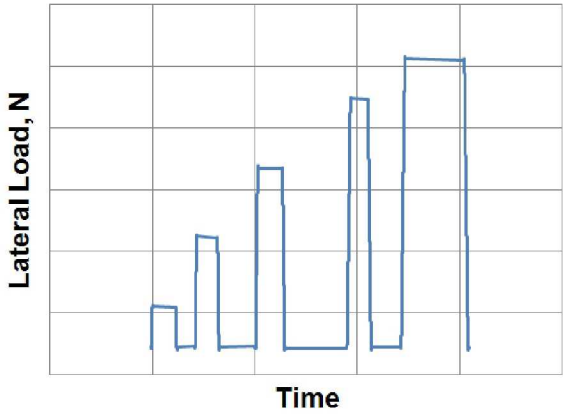

Figure 11. Load Case 2 Time History. *This plot shows application of constant rate lateral load ramps with variable inspection hold times at loaded and unloaded states for the Load Case 2 loading sequence; the final ramp shown is the maximum expected mission lateral load.*

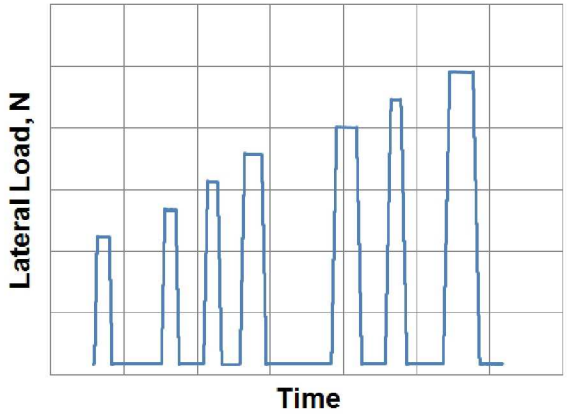

Figure 12. Load Case 3a Time History. *This plot shows application of constant rate lateral load ramps with variable inspection hold times at loaded and unloaded states for the Load Case 3a loading sequence; all ramp peaks are at magnitudes greater than the maximum expected mission lateral load.*

The data plots of Load Case 3a initially replicates Load Case 2, as the increased lateral load ramps of this case are an experimental extension of the Load Case 2 ramps. Fig. 12 provides the load-time history for the seven increasing peak lateral load ramps of Load Case 3a; the last peak value was more than twice the Load Case 2 lateral load value. For the Load Case 3a loadings, the accumulation of inelastic deformation and strain (Figs. 13 to 15) is evident, as described in the Material Inelasticity Description (Section B) above. The average lateral deflections shown in Fig. 13 were measured from the "X" axis of the upper and lower deflection plates (shown in Fig. 4), denoted by "UX" and "LX". For Fig. 14 and the remaining lateral rotation figures, the total rotation, CSAF rotation (ΘROT), and heater head rotation (ΘBEND) are shown. Even at the maximum lateral load of this case, the measured residual strain at the high stress area remained well below 0.2%, so it is assured that the defined yield strength (0.2% offset) was not reached. In addition, no other failure modes were observed for Load Case 3a. The peak load of Load Case 3a was slightly greater than the predicted load to reach the defined yield stress at the most critical location of the test article.

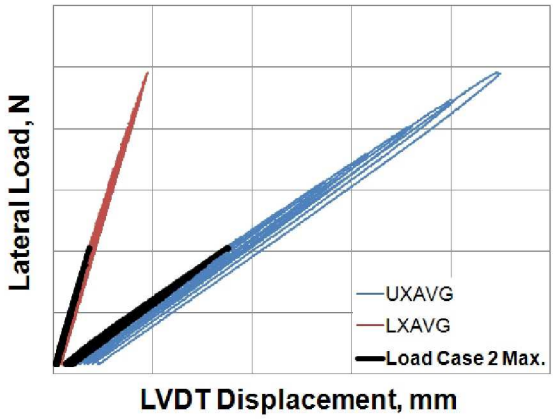

Figure 13. Load Cases 2 and 3a Measured Lateral Deflections. *For the prefailure lateral load cases, the measured lateral deflections closely matched the predicted values, especially after the first 20 to 30% of the maximum load shown. Very little inelastic behavior is noted at and below the maximum expected mission lateral load shown in bold.*

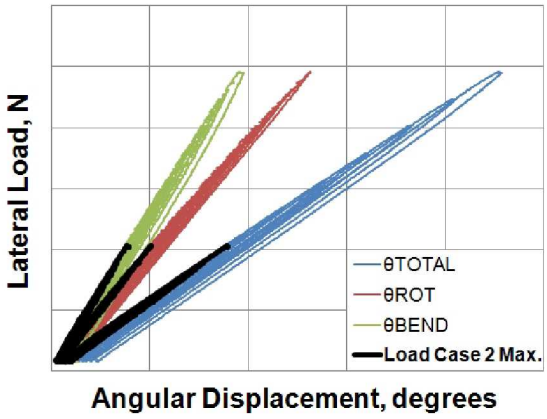

Figure 14. Load Cases 2 and 3a Measured Lateral Rotations. *Similar to lateral deflections measured for the prefailure lateral load cases, the measured lateral rotations matched the predicted values. Again, very little inelastic deformation is apparent at and below the maximum expected mission lateral load shown in bold.*

E. Load Case 3b

To determine the maximum lateral load-carrying capacity of the test article and induce gross structural deformation or other failure modes, the internal pressure and axial compressive loads were maintained as in Load Cases 2 and 3a, and a final lateral load ramp using the constant rate from previous testing was imposed on the test article. The end peak load for this ramp was set to a very high value to cause test termination by attaining a predefined large lateral deflection. The load-time history for Load Case 3b is shown in Fig. 16, where a peak load was reached that is more than three times greater than the maximum expected mission lateral load. Lateral deflections (Fig. 17), lateral rotations (Fig. 18), and longitudinal strains (Fig. 19) were linear up to the magnitude of the peak lateral load of Load Case 3a, and then followed an elastic-plastic curve that may be typical for the MarM-247 heater head material. The average lateral deflections shown in Fig. 17 were measured from the "X" axis of the upper and lower deflection plates (shown in Fig. 4), denoted by "UX" and "LX". The linear response of the lower deflection plate indicated that the CSAF remained elastic, while the large nonlinear deformation measured at the upper deflection plate, as well as visual inspection of the test article, revealed formation of a plastic hinge at the heater head high stress areas.

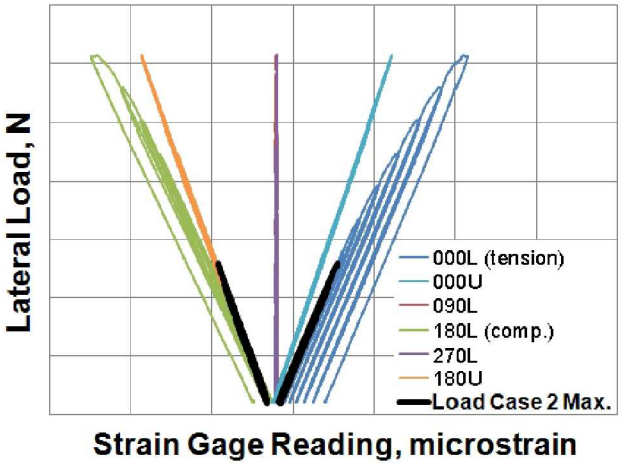

Figure 15. Load Cases 2 and 3a Measured Longitudinal Strains. *Longitudinal strains measured at predicted peak stress locations were linear and elastic at and below the maximum expected mission lateral load shown in bold. At higher lateral loads, inelasticity is evident on the bending tensile side (000L) and, to a lesser extent, the bending compressive side (180L).*

The failure mode achieved in Load Case 3b was yielding of the heater head and resultant gross deformation. Upon physical inspection after completion of Load Case 3b, no other failure modes were evident.

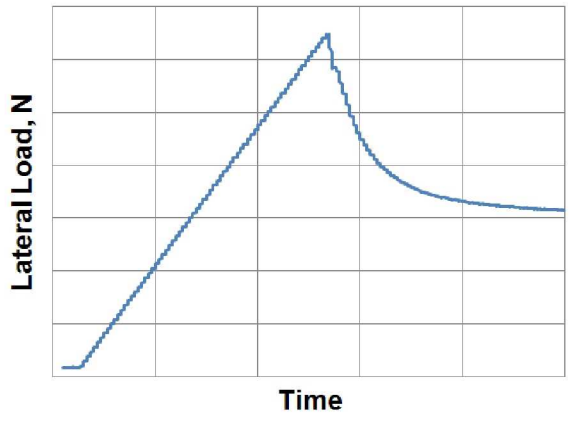

Figure 16. Load Case 3b Time History. *This plot shows application of a constant rate lateral load ramp until failure of the test article is manifest, when the test load frame automatically shut down and released the load. The peak lateral load attained was more than three times the maximum expected mission lateral load.*

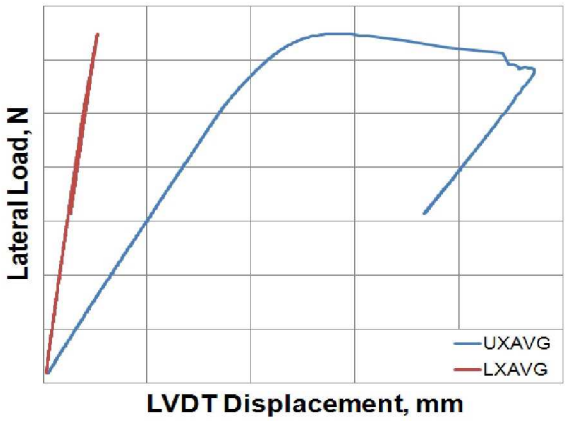

Figure 17. Load Case 3b Measured Lateral Deflections. *The measured lateral deflections for the failure load case indicated that the CSAF remained linear and elastic, while the heater head yielded considerably without losing pressure integrity.*

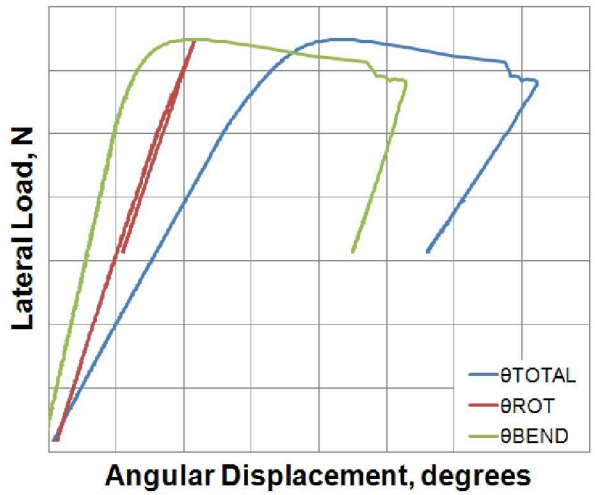

Figure 18. Load Case 3b Measured Lateral Rotations. *Similar to the measured lateral deflections, the lateral rotation measurements for the failure load case indicated that the CSAF remained linear and elastic, while the heater head yielded considerably.*

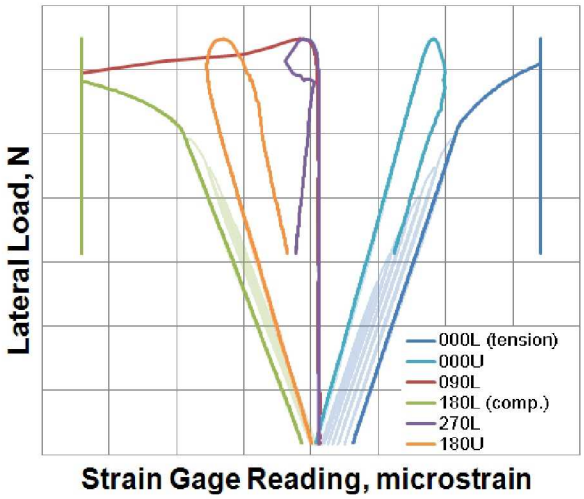

Figure 19. Load Case 3b Measured Longitudinal Strains. *Even at the highest stress area, the longitudinal strains under the failure lateral loading were linear up to prior history load levels (shown in phantom), then followed the shape of a stress-strain curve typical for the heater head MarM-247 material.*

V. Conclusion

The Heater Head Lateral Load Test was successful in directly supporting qualification of the Advanced Stirling Convertor (ASC)–E2 heater head analysis and validation of the design to meet launch requirements. The pressurized test article was exposed to anticipated maximum axial compressive and maximum lateral loads during an Advanced Stirling Radioisotope Generator (ASRG) launch, and reliably sustained these load conditions. After demonstrating that the test article did not fail under flight-like loads, the test continued with increased lateral loading until the heater head yielded, sustaining more than three times the maximum expected mission lateral load while maintaining pressure integrity. This test result validated the capability of the heater head to meet the launch load requirements with sufficient margin.

Acknowledgments

This work is funded through the NASA Science Mission Directorate. Any opinions, findings, and conclusions or recommendations expressed in this article are those of the authors and do not necessarily reflect the views of the National Aeronautics and Space Administration. The authors wish to acknowledge the people who made this effort possible including Jeff Schreiber, Ralph Pawlik, Wayne Wong, Frank Bremenour, and Sreeramesh Kalluri of NASA Glenn Research Center, as well as Debbie Kuhlman and Greg McNelis of Lockheed Martin for their counsel and support throughout this test. The authors also thank Ms. Angela Coates of the University of Akron for her real-time evaluation of test article response and enthusiastic analysis of the voluminous post-test data.

References

[1]Chan, J., Wood, J.G., and Schreiber, J.G., "Development of Advanced Stirling Radioisotope Generator for Space Exploration," proceedings of Space Technology and Applications International Forum (STAIF 2007), edited by M.S. El-Genk, AIP Conference Proceedings 880, pp. 615–623, 2007.